European Commission

JRC TECHNICAL REPORTS

Revised Black Sea ecosystem model

Svetla Miladinova
Adolf Stips
Diego Macias Moy
Elisa Garcia-Gorriz

2017

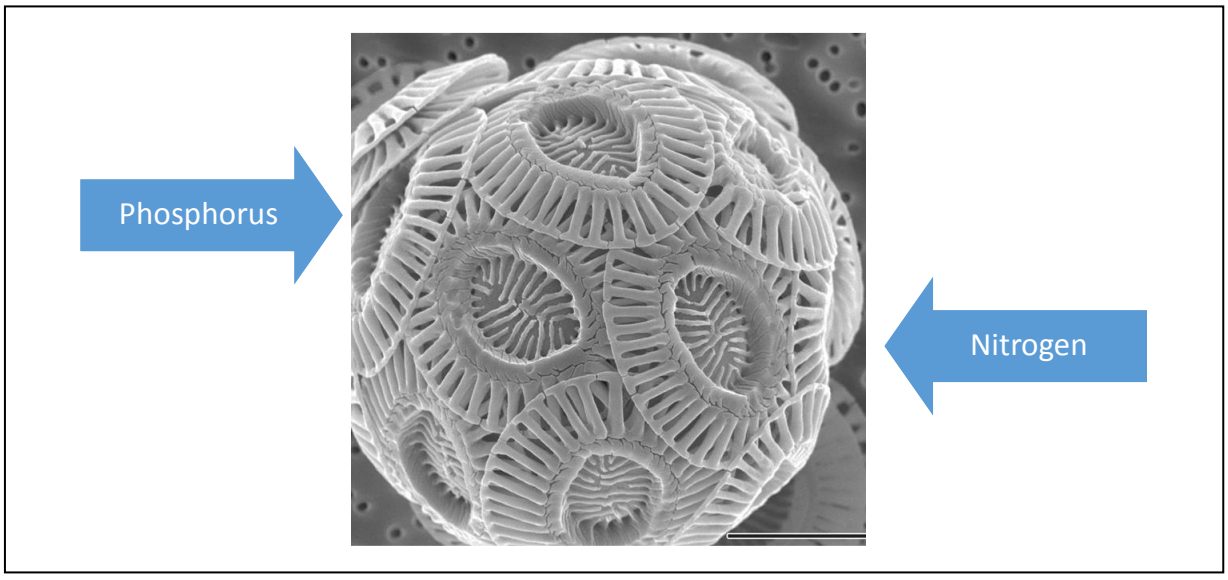

Joint Research Centre

EUR 28983 EN

Revised Black Sea ecosystem model

Contact information
Name: S. Miladinova
Address: Joint Research Centre, Via E. Fermi, 2749 – TP27, 21021 Ispra (VA), Italy
E-mail: svetla.miladinova@ext.ec.europa.eu
Tel.: 6277

JRC Science Hub
https://ec.europa.eu/jrc

JRC 109702

EUR 28983 EN

ISBN 978-92-79-77212-2

ISSN 1831-9424

doi:10.2760/220233

How to cite: Svetla Miladinova, Adolf Stips, Diego Macias Moy, Elisa Garcia-Gorriz; Revised Black Sea ecosystem model; EUR 28983 EN; doi:10.2760/220233

Table of contents

Acknowledgements

We acknowledge Prof. Temel Oguz for making available the basic structure of the BSEM model. Special thanks go to the GETM, GOTM and FABM developers for providing and maintaining the model.

Abstract

The regional Black Sea Ecosystem Model (BSEM) has been updated to describe better the Black Sea phytoplankton growth specific features, like the strong winter-spring blooms followed by usually less intense blooms in fall. The revised BSEM model includes a phosphorus cycle in order to explore variability of phytoplankton blooms under phosphorus limitation.

Two specific features of the upper layer water-column physical and biogeochemical structures have been addressed in the present study.

- A detailed view of the large- and mesoscale-circulation characteristics, and thus more detailed interpretation of the spreading and mixing of nutrients is achieved by the use of tracer model simulations. They give us knowledge on the spreading of nutrients and biological matter, coming from the main Black Sea rivers, deep basin pool and intermediate layers, respectively, to the euphotic zone.

- BSEM model calibration with constant and variable phosphorous/nitrogen ratio is performed. The relative importance of both fertilizers (nitrate and phosphate) on the phytoplankton growth is shown.

1. Introduction

The Black Sea's ecosystem has experienced substantial changes since the 1960s, such as nutrient enrichment and large population growth of gelatinous and opportunistic species (Daskalov, 2003). Most likely excessive anthropogenic nutrient loading and overfishing contributed to this ecological degradation. Compared to other European seas, the nutrient inputs to the Black Sea are high. For instance, the total nitrogen input in the 1990s to the northern part of the Black Sea alone is six times that of the Baltic Sea and more than twice as high as the input to the North Sea. River export of total phosphate to the coastal waters of the northern part of the basin is comparable to that transported to the Baltic Sea, but lower than loads exported to the North Sea (Artioli et al. 2008). However, trends in the phytoplankton growth over time in the shelf as well in the deep basin remain an issue of discussion (Yunev et al., 2014). The annual cycle of phytoplankton in the Black Sea has been widely studied but most of the studies considered coastal or shelf areas (see reviews in Sorokin, 2002; Nesterova et al., 2008) and only a few the deep waters. A specific characteristic of the seasonal phytoplankton dynamics is a usually excessive phytoplankton bloom in winter. This pattern is not typical for temperate seas, where the perceptible spring phytoplankton bloom follows the low winter phytoplankton biomass (Nezlin, 2008; Finenko et al., 2014). Despite this well-known property of the seasonal phytoplankton dynamics in the Black Sea, there has not a good theoretical explanations for this phenomenon (Mikaelyan et al., 2013).

Our primary aim is to study the main physical and biological processes that control the seasonal cycle of the plankton dynamics over the entire Black Sea. This study focus is on the key processes that determine the yield gradient from the coastal river influenced areas to the open sea. A three-dimensional, low-trophic level, coupled biophysical model for the Black Sea ecosystem (BSEM) is developed in the framework of the SIMSEA project (Miladinova et al., 2016 a, b, c). The uncertainties related to the parameterisation of biological processes along with the low temporal and spatial coverage of observations are the main challenges concerning the calibration and validation of BSEM.

Usually two nutrients in human-derived sources, phosphorus (P) and nitrogen (N), are of most concern in eutrophication. N is often the nutrient that first limits primary production of photosynthetic organisms in many temperate marine waters (Moore et al., 2013). Available nutrient data (Basturk et al., 1997) indicated strong nitrogen limitation in the Black Sea euphotic zone waters of the interior basin, since the $N:P$ ratio is typically less than 8 (Oguz, 2005). P can limit or co-limit algal growth in coastal and shelf zones that are sustaining high N inputs (Tsiaras et al., 2008, Oguz and Ediger, 2006). According to the data shown in Oguz (2005), inner shelf waters of the north-western Black Sea may have been under co-limitation by phosphorus, and nitrogen depending on local conditions (the $N:P$ ratio is about 20 or even 40). If the biogeochemical model considers both limiters (nitrate and phosphate), corresponding reductions in the shelf and coastal phytoplankton blooms will allow more inorganic N to be transported to the basin interior where it can support larger blooms. Both N and P are considered here, and these nutrients should be co-managed in the development of strategies to minimize the eutrophication.

Recent surveys of $N:P$ into the phytoplankton cells (Martiny et al., 2013; Galbraith and Martiny, 2015) and nutrient tracers (Teng et al., 2014) show that this ratio shows systematic variations throughout the ocean: with $N:P>20$ in subtropical seas and $N:P<12$ in high-latitude regions. These patterns are not yet fully clarified, but appear to fundamentally change our understanding of the relationships between nutrient cycles and how they influence net primary productivity, carbon export, and deep ocean nutrient inventories.

Another aim of the study is to improve the BSEM model (Miladinova et al., 2017) by including the phosphate as a state variable and further allowing the $N:P$ ratio to variate

with the nutrient content. Finally, the relative importance of both fertilizers (nitrate and phosphate) on the Black Sea ecosystem development is discussed.

2. Materials and Methods

2.1 Study area

The Black Sea is characterised by large spatial heterogeneity of biological and hydro-chemical characteristics (Konovalov and Murray, 2001; Yunev et al., 2007; Miladinova et al., 2017). Hence, seasonal and long-term variability of phytoplankton growth and distribution can be examined separately for the inner part of the basin with depth 1500m, for the shelf slope 200-1500m, and North western Shelf (NWS) and coastal regions (Fig. 1). These regions are selected on the basis of several Black Sea characteristics, like bathymetry, currents and riverine influence (Miladinova et al., 2016 a, 2017).

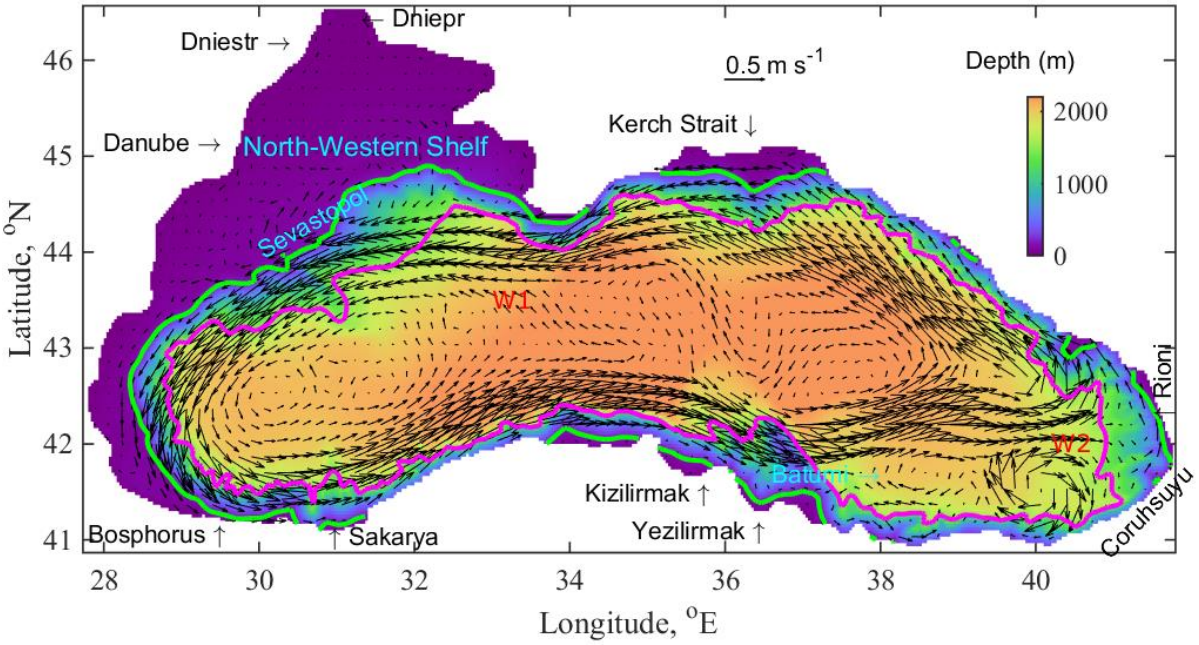

Figure 1. Bathymetry and location map of the Black Sea, main rivers and locations of Batumi and Sevastopol anticyclonic eddies. The 1500 m is drawn in magenta and the 200 m isobath is given in green. Simulated climatological velocity vectors at 5 m depth in September, averaged over 1991-2015, are presented by black arrows. W1 and W2 are the locations of the two points, where surface salinity from the WOA13 (https://www.nodc.noaa.gov/) is extracted.

2.2 Models

A model capable to simulate the mesoscale circulations and thermohaline structure in the Black Sea for a continuous multi-decadal period without any relaxation towards external fields is used (Miladinova et al., 2017). This 3D hydrodynamic model comprises the 3D GETM (http://www.getm.eu/) and the General Ocean Turbulence Model (GOTM). Turbulence is modelled with a two-equation turbulence model; one equation for the turbulent kinetic energy and one equation for the dissipation rate of the turbulent kinetic energy. The model includes a simple parameterisation of deep-water mixing. In order to parameterise unresolved turbulence production by internal wave shear, internal wave

breaking or Kelvin–Helmholtz instability under stably stratified conditions (Burchard et al., 2006), a lower limit to the turbulent kinetic energy is set ($k_{\min}$ =const). In this study the minimum turbulent kinetic energy, $k_{\min}$, has been changed to increase the mixed layer depths and decrease the surface salinity oscillations. Long-term evolutions of annual sea surface salinity (SSS) from four runs averaged for the deep interior basin are shown in Fig. 2 together with WOA13 10-year mean SSSs at W1 and W2 (see Figure 1 for their locations). When $k_{\min}$ is set to low value (5.10^{-7} m^2 s^{-2}), then SSS begins to decrease steeply since 1962 and the run has been terminated in 1971. In Miladinova et al. (2017) the value of 10^{-6} m^2 s^{-2} has been used. In addition, in Miladinova and Stips (2010) the best fits for nutrients in the Baltic Sea were found in the interval $6.10^{-7} < k_{\min} < 8.10^{-7}$ m^2 s^{-2}. A small decrease of $k_{\min}$ (from 10^{-6} m^2 s^{-2} to 9.10^{-7} or 7.10^{-7} m^2 s^{-2}) decreases the turbulent mixing and the oscillations in the surface salinity are dampened. The best fit for salinity distribution in the Black Sea is estimated to be 7.10^{-7} m^2 s^{-2}. Model ability to represent reasonably salinity variation in time and space is a key factor for successful representation of nutrient distributions. Further, the short wavelength radiation coefficient (A) is changed from 0.95 to 0.9 and a weak surface zooming (ddu=2) is applied (see Miladinova-Marinova et al., 2016 a). The coefficient A was higher in the pure hydrodynamic simulation in order to parameterise the organic matter shading effect. In the coupled biogeochemical and hydrodynamic model a feedback between the organic matter and water optical depth is considered. The model has been improved to match better the experimental evidence.

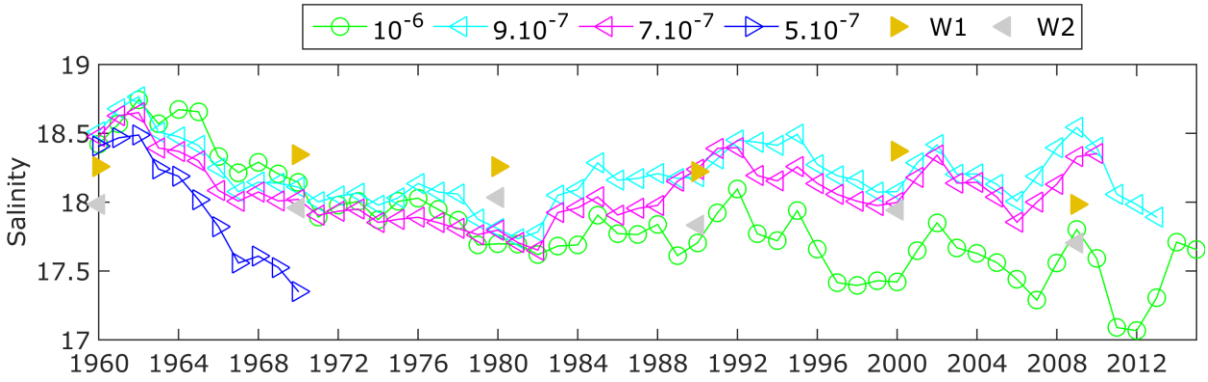

Figure 2. Variations of annual SSS averaged over the interior basin with depth greater than 1500 m from four different simulations (values of $k_{\min}$ (m^2 s^{-2}) used in the simulations are given in the legend). WOA13 (https://www.nodc.noaa.gov/OC5/woa13/) 10-year mean SSS at locations W1 and W2 (Figure 1) are given with filled triangles.

A passive tracer model is linked via the Framework for Aquatic Biogeochemical Models (FABM, Bruggeman and Bolding, 2014) with the hydrodynamic model. Three different simulation runs are done by using the passive tracer model.

The resultant flow fields from the hydrodynamic model are also used to calculate the evolution of the low trophic level components of the food chain in the Black Sea ecosystem (Miladinova et al., 2016 c). To describe the low trophic level pelagic ecosystem of the Black Sea, a nitrate-based biogeochemical model has been implemented following the existing literature (Oguz et al., 1999, 2000, and 2014). This model provides an optimally complex system of food web interactions and biogeochemical cycles comprising oxic-, suboxic- and anoxic waters of the Black Sea. It represents the classical omnivorous food-web with 7 state variables. These include two phytoplankton size groups (small and large), four zooplankton groups including micro- and mesozooplankton, non-edible dinoflagellate species as Noctiluca, and the gelatinous zooplankton species Mnemiopsis. The three most

dominant phytoplankton taxonomic groups observed in the Black Sea like Bacillariophyta (diatoms), Dinophyta (dinoflagellate) and Chrysophyta (coccolithophore E. huxleyi, see picture on the front page) comprise the large phytoplankton group. Phytoflagellates and picophytoplankton constitute the smallest members of the observed community structure. They are included as the small-size phytoplankton compartment into the model. All plankton biomass are expressed in nitrogen units, since the nitrogen is considered to be the most important limiting nutrient for the interior Black Sea ecosystem (Oguz and Merico, 2006). Nitrogen is represented by two inorganic nutrients (nitrate and ammonium) and included in the particulate organic material (detritus). Additional state variables are dissolved oxygen and hydrogen sulphide. This system offers an optimal complexity with medium complex trophic interactions. The full set of equations describing this ecosystem is given in Miladinova et al. (2016c).

BSEM model has been rigorously and precisely verified and validated against measured data and independent calculations (Miladinova et al., 2016 b and Miladinova et al., 2017). The numerical experiments indicate that the biogeochemical components of the model adequately reproduce the main features and state variable evolution in the Black Sea ecosystem: the growth in phytoplankton biomass and changes in seasonal cycles of the main ecosystem components. It is furthermore shown, that the physical processes are of fundamental importance for a reliable reproduction of seasonal and inter-annual changes in the ecosystem. When model simulations are compared with the CMEMS satellite data, the BSEM model usually gives an overestimation of about 0.5 mg Chl m^{-3} in the northern and southern shelf areas, as well as along Rim current meandering in the western basin. In the current BSEM model only nitrogen limits the primary production, however there are several occurrences that maybe the phosphorus is limiting the phytoplankton growth, too. For example, an intense bloom of coccolithophores were observed in several years when the $N:P$ ratio was low. The increase of $N:P$ ratio above the Redfield stoichiometry led to the domination of the diatoms in phytoplankton community (Silkin et al., 2014). Various amounts of a nitrogen and phosphorus sources into marine water appear to be essential precondition for phytoplankton growth. Therefore a model update to include phosphate as a state variable is required.

2.3 BSEM update

The basic set of BSEM equations can be find in Miladinova et al. (2016c), where here we present only the recent model updates. The main change in the model consists of adding phosphate as limiting the primary production. Thus, a new state variable, PO , is introduced into the model. The new limitation function of the primary production is as follow

$$\Psi_X = \sigma_X \cdot f_X(N_n, N_a, PO) \cdot f_X(I) \cdot f_X(T) , \qquad (1)$$

where σ_X , denotes maximum specific growth rates at 20°C, $f_X(I)$, the limitation function due to light, and $f_X(T)$ the limitation function due to temperature (Miladinova et al. 2016c). Function Ψ_X represents the growth rate, N_a and N_n denote ammonium and nitrate concentrations, respectively, and the subscript *X* denotes either *L* for the large or *S* for the small size group. The principal difference between Ψ_X in BSEM version described in Miladinova et al. 2016c and eq. 1 consists of limitation function depending on PO . The function $f_X(N_n, N_a, PO)$ is parameterised assuming that either N or P controls phytoplankton growth (Oguz and Merico, 2006). This function represents the nutrient uptake expressed as the minimum of total nitrogen (sum of nitrate and ammonium) limitations $f_X(N_n, N_a) = f_X(N_n) + f_X(N_a)$ and phosphorus limitation $f_X(PO)$ .They are expressed by the Monod-type hyperbolic functions involving a saturation response at high resource concentrations

$$f_X(N_a)=\left[\frac{N_a}{K_{AX}+N_a}\right],\quad f_X(N_n)=\left[\frac{N_n}{K_{NX}+N_n}\right]\cdot\exp(-\lambda\cdot N_a),\quad f_X(PO)=\left[\frac{PO}{K_{POX}+PO}\right] \quad (2)$$

where $K_{NX}=a+bP_X$, $K_{AX}=0.1K_{NX}$ and $K_{POX}=K_{NX}/np$ are the corresponding half saturation functions of nitrate, ammonium and phosphate uptakes. They are parameterised following Tsiaras et al., (2008). Values of the constants a , b and λ are given in Table 1, while the denominator np represents the $N:P$ ratio. The nitrogen limitation function is based on Wroblewski (1977) and accounts for the inhibition of nitrate uptake in the presence of ammonium. Following Liebig's law of the minimum, the nutrient uptake rate is thus limited by either total nitrogen or phosphorus.

Thus the growth rate, Ψ_X , that limits the primary production is defined by

$$\Psi_X=\sigma_X\cdot f_X(I)\cdot f_X(T)\cdot\min\left\{f_X(N_a)+f_X(N_n),f_X(PO)\right\}. \quad (3)$$

Available data (Oguz and Merico 2006; Oguz and Ediger, 2006; Tugrul et al., 2014) indicates a broad regional change of the $N:P$ ratio. In particular, this ratio is small in the inner part of the basin and large on the NWS and coastal areas. The ratio changes along the water column, too. It is higher in the Cold Intermediate Layers (CIL) than in the upper layers (Mikaelyan et al., 2013). The elemental ratios of nitrogen, phosphorus, and carbon in marine phytoplankton can diverge significantly from the Redfield ratio, but the underlying reasons have been hard to explain. As a result, many biogeochemical models often ignore this stoichiometric variability. We are checking the model performance by applying np = const or using a simple relationships between $N:P$ ratio and dissolved phosphate concentration (Martiny et al., 2013)

$$np=140/\left[6.9PO+6\right] \quad (4)$$

Changes in phosphate concentration are expressed by

$$R(PO)=\left\{\varepsilon_n D_n+\sum_k \mu_{zk}\cdot Z_k-\left[\sum_k \Psi_k\cdot P_k\right]\right\}/np\,. \quad (5)$$

Only one compartment for the biogenic detritus, D_n , is involved since the detritus decomposition rate for phosphate is assumed to be the same as for nitrate. So, the equation (5) is similar to the nitrogen based equations except it is divided by the assumed biomass stoichiometry np .

The temperature control of the growth, $f_X(T)$ for the large phytoplankton is set to 1, while for the small phytoplankton

$$f_S(T)=Q_S^{(T-20)/10}. \quad (6)$$

In this way the grow rate of large phytoplankton group is not pushed to grow fast at low temperatures (Miladinova et al. 2016c). Weak temperature control is imposed for the small phytoplankton group, however the lower growth rate of the large phytoplankton group gives indirectly the small phytoplankton group a growth advantage.

Mineralization rate depends on temperature

$$\varepsilon_n=\varepsilon_{n0}\exp(c_1 T), \quad (7)$$

where ε_n (d^{-1}) is the remineralisation rate of detritus (see Eqs. A9a, b and A11c in Miladinova et al. 2016c), ε_{n0} (d^{-1}) is the default remineralisation rate and c_1 is a constant.

Next update includes a sinking speed of the large phytoplankton (see Table 1).

Table 1. New or modified BSEM input parameters as they are listed in the "fabm.yaml" FABM input file.

Parameter	Value	Unit	Definition	Default
sfl_po	0.005	mmol $Pm^{-2}d^{-1}$	Constant surface nitrate flux	0.083
kp	0. 1	m^2 (mmol N) $^{-1}$	Phytoplankton self-shading coefficient	0.07
kd	0.06	m^2 (mmol N) $^{-1}$	Detritus self-shading coefficient	0.06
ka_l	0.1		Half-saturation constant for ammonium uptake from large phytoplankton	0.1
ka_s	0.1		Half-saturation constant for ammonium uptake from small phytoplankton	0.1
a_n	0.5	mmol N m^{-3}	First half-saturation constant for nitrate	0.5
b_n	0.5		Second half-saturation constant for nitrate	0.5
a_pl	3.0	(mmol N) $^{-1}$	Ammonium inhibition parameter for large phytoplankton	3.0
a_ps	3.0	(mmol N) $^{-1}$	Ammonium inhibition parameter for small phytoplankton	3.0
sink	-5.0	m d^{-1}	Detritus sedimentation rate	-5.0
w_pl	-0.5	m d^{-1}	Phytoplankton sedimentation rate	-0.5
s1	0.15		Temperature factor of mineralisation	0.15
s2	0.1	mmol N m^{-3}	Detritus limit	0.1
np	16		Phytoplankton N:P stoichiometry	16
Q10pl	1		Temperature control of large phytoplankton	2
Q10ps	2		Temperature control of small phytoplankton	2
Q10zl	2		Temperature control of large zooplankton	2
po	1.5	mmol P m^{-3}	Phosphate	0.5

2.4 Model forcing and setup

The quality of the forcing data affecting our simulations has been analysed in Miladinova et al. (2016a, b) and the most appropriate hydrodynamic forcing data capable to assess the potential changes in the Black Sea dynamics has been selected.

Table 2. Summary of tracer setup configurations.

Tracer runs	TR1	TR2	TR3
Starting year	1960	1960	1960
End year	2015	2015	2015
Initialisation month	January	December	December
Initialisation area	NWS (depth<200m)	Inner basin (depth>1500m); From 200m to the bottom	Inner basin (depth>1500m); See Fig. 3a
Concentration (mmol m^{-3})	1	1	$0 \div 7.5$

The summary of the tracer setup configurations is given in Table 2. The first tracer run (TR1) is used to identify paths of the NWS water mases through the entire basin in a particular year. In the beginning of each simulation year the NWS with depth less than 200 m is filled with a tracer concentration 1 (mmol m^{-3}), while in the rest of the basin the tracer concentration is 0. The run has been always initialised in the beginning of the year. The second run (TR2) is designed to visualise the process of nutrient uplift from the pool to the euphotic zone, both in time and space. For this reason the inner part of the basin with depth greater than 200 m is filled with a tracer concentration 1 (mmol m^{-3}) from 200 m until the bottom, while in the upper 200 m the tracer concentration is 0. The third run (TR3) is intended to show the mixing of the intermediate layer with high nitrate concentration (Tugrul et al., 2014), which is called further nitrate storage. During winter convection, the bottom-up flux of nitrate from the CIL and the upper part of the main pycnocline transports nitrate to the euphotic zone (Oguz, 2005; Yunev et al., 2005). The third run is initialised with the nitrate initial profile for the basin inner part with depth higher than 1500 m (Fig. 3). The second and third runs have been initialised in December.

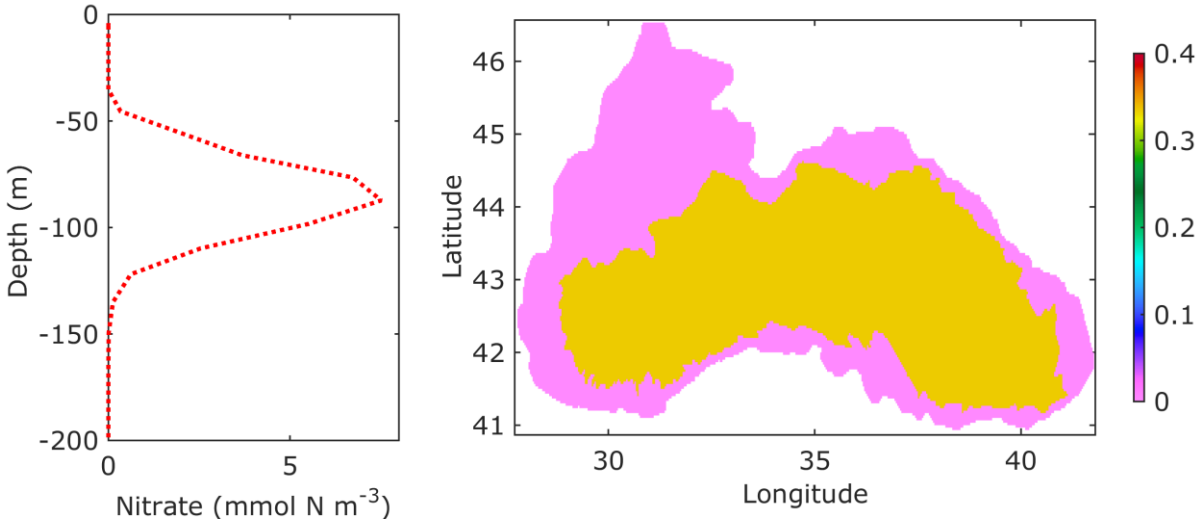

Figure 3. Nitrate (mmol N m^{-3}) initial vertical profiles (left) and horizontal slice at 45 m (right).

River nutrient load data is issued from the SESAME and PERSEUS projects (Ludwig et al., 2009). In Fig. 4 are given the annual mean nitrate phosphate fluxes from the Danube. Due to the lack of consistent data, climatological values are used since 2000. Further improvement of the river nutrient loads is required in order to match the observed chlorophyll data and to maintain the long-term simulations.

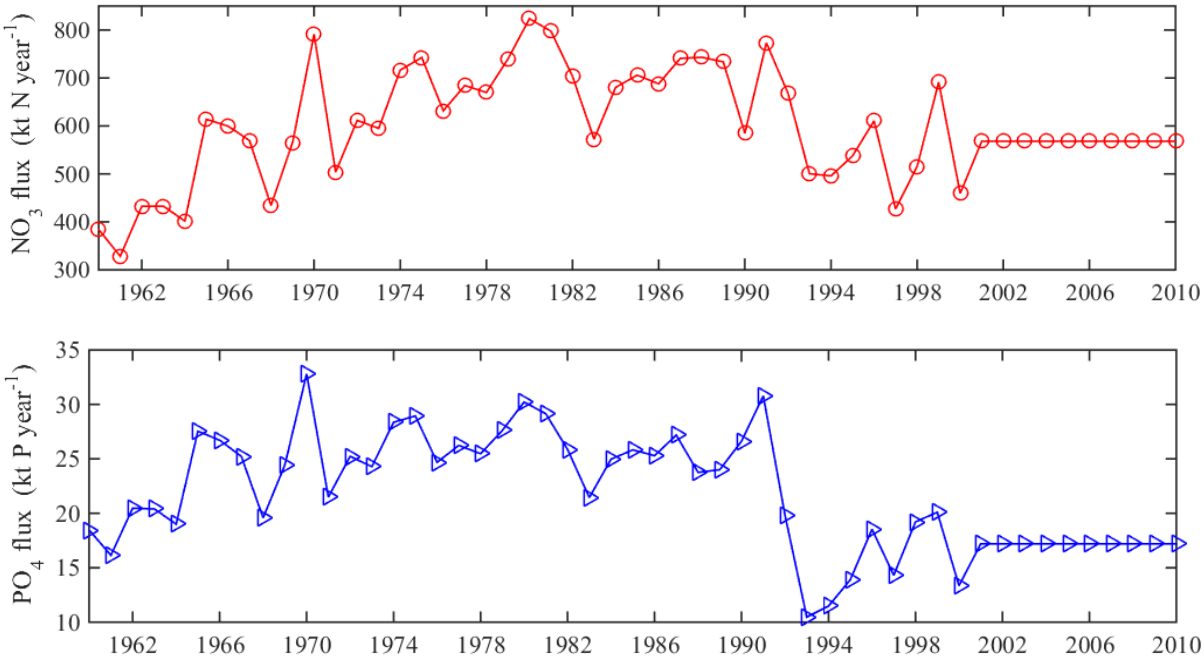

Figure 4. Annual mean nitrate and phosphate fluxes from the Danube River.

Model calibration shows that nutrient initial storage in the intermediate and deep layers are very important part of the model setup since it can support the phytoplankton growth for a long time even without load from rivers. Due to the lack of available nutrient climatology for the Black Sea, the initial conditions of the BSEM variables are arranged to be similar to Knorr 2001/2003 experimental data (Cannaby et al., 2015; Tugrul et al., 2014; Stanev et al., 2014). They reproduce mainly the observed characteristics near north-western and south-western shelf of the Black Sea ecosystem during spring. Nitrate concentration is set to 0.33 mmol N m^{-3} within the upper 10 m, then it increases to 3.7 mmol N m^{-3} between 15 m and 35 m depths and decreases to zero at 100 m. Ammonium is set to 0.03 mmol N m^{-3} within the upper 90 m, then it increases linearly to 70 mmol N m^{-3} between 90 m and 450 m depths and remains constant till the sea bottom. Hydrogen sulphide is zero in the upper 90 m, then it increases linearly to 860 mmol HS m^{-3} at the sea bottom. Dissolved oxygen decreases linearly from 340 mmol O_2 m^{-3} to 0 in the upper 70 m and is set to zero further below. All the other BSEM state variables are set to small and vertically uniform values over the entire water column because their equilibrium structures do not depend on the initial conditions and are emergent properties of the model dynamics.

3. Results and verification

3.1 Tracer model simulations

The distributions of hydro-chemical properties in the upper layer appear to be sensitive to external pressures originating from regional weather variability (Konovalov and Murray, 2001; Oguz and Velikova, 2010) and anthropogenic inputs (Kıdeyş, 2002; Mee, 1992;

Oguz, 2008). These distributions are influenced by the surface circulation, which is dominated by basin wide cyclonic current (the Rim Current), leading to formation of two quasi-permanent cyclones or gyres in the interiors of the eastern and western basins and a series of anticyclonic eddies within the Rim Current along the coastal margin (Oguz et al., 1992; Özsoy and Ünlüata, 1997). It is recently found the Black Sea circulation system to involve a spatially complex structure dominated by mesoscale features instead of a simple twin-gyre, quasi-permanent circulation (Korotaev et al., 2003; Kubryakov and Stanichny, 2015; Miladinova et al., 2017). The effect of this mesoscale-dominated circulation system on material transport across the basin is observed to be significant (Oguz et al., 2004). Tracer simulations are performed to foresee the spreading of nutrients and biological matter coming from the rivers, deep basin pool and intermediate layers to the euphotic zone.

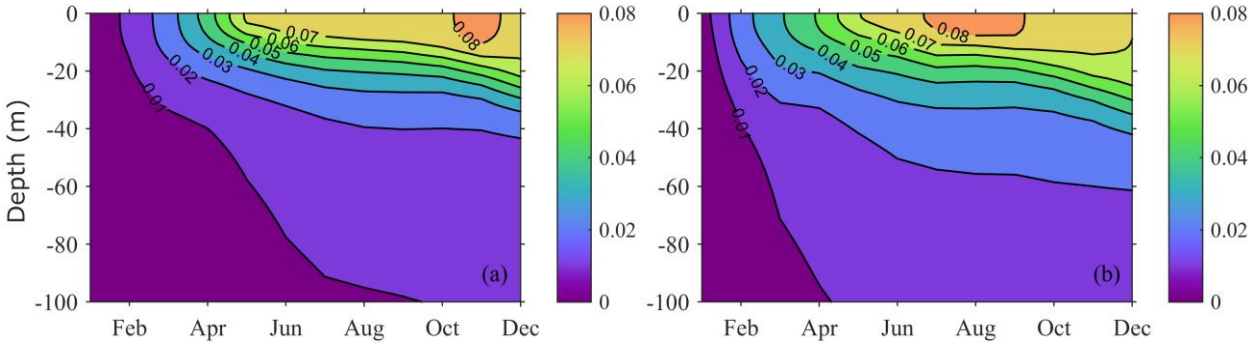

Figure 5. Deep basin climatological contours of TR1 (a) for 1960-1970 and (b) for 1971-1995.

Nutrients coming from the three big rivers in the NWS (see Fig. 1) are the main source of anthropogenic load to the Black Sea. TR1 run is dedicated to represent the spreading of the NWS nutrients, which are not utilised by the phytoplankton on the shelf and coastal zones. Mostly nitrate can be in excess due to its high concentrations in these zones and the phosphate limiting growth of the phytoplankton (Tsiaras et al., 2008, Oguz and Merico, 2006; Mikaelyan et al., 2015). The deep basin (with depth > 1500m) climatological contours of TR1 are shown in Fig. 5 for two distinct periods: (a) for 1960-1970 and (b) for 1971-1995. The periods are selected based on the already identified break points (Miladinova et al., 2017 b). Generally, TR1 is spread in the near-surface layers of the basin interior from February to April. In the first period (Fig. 5a), the mixing period begins later and it lasts in shorter period, as the strongest TR1 gradients have occurred in March-April. On the other hand, the tracer penetration into the intermediate layers is weaker than in the second period (Fig. 5b). Despite the differences in the distribution, nutrients coming from the big rivers on the NWS contribute mostly to the late-spring and early-summer phytoplankton blooms for both time periods. Such blooms are frequently observed in the Black Sea (Oguz and Ediger, 2006).

The vertical chemical zonation in the Black Sea results from the strong vertical density gradient in the water column. Most of the biogeochemical processes take place within the uppermost 100 m of the water column. The euphotic zone structure, covering maximally the uppermost 75 m (approximately). The underlying 20-30 m layer contains steep gradients in chemical properties where particle remineralization causes considerable reduction in oxygen concentration to the values of approximately 10 mmol m^{-3}, whereas nitrate increases to maximum concentrations of 6-9 mmol m^{-3} (within the nitrate storage), followed by the rapid decrease of nitrate concentrations to zero due to the consumption in organic matter decomposition (Murray, 2006). Below, sulphate is used to decompose organic matter, and hydrogen sulphide is produced as a by-product. The pool below 100 – 200 m (almost pycnocline) is full with ammonium (about 100 mmol N m^{-3}) and

phosphate (about 6 mmol P m^{-3}). The mechanism of nutrient uplift from the pycnocline (150 – 200 m) to the euphotic zone is unclear as well as the reason for the strong winter phytoplankton bloom in the Black Sea (Mikaelyan et al., 2017).

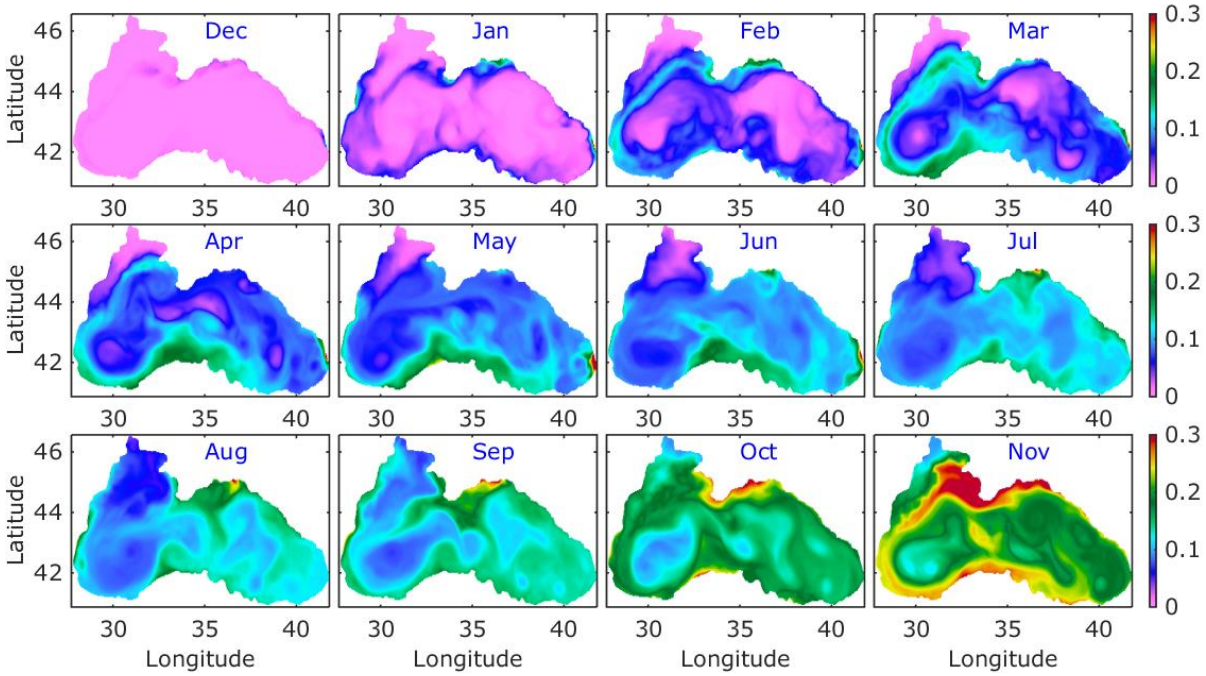

Figure 6. Climatological monthly distribution of TR2 from 1960 to 1990.

TR2 displays the lifting of nutrients from water levels deeper than 200 m below the surface to the surface layers. In Fig. 6 the climatological monthly distribution of TR2 from 1960 to 1990 is presented. TR2 is averaged over the upper 10 m. The model run is initialised in the beginning of each December. In January the tracer can be perceived in coastal zones, despite the fact that these zones are not included in the tracer initialisation (i.e. TR2=0). In February 0.1 of the tracer is well noticed in the Rim Current area and tracer concentration is further increased in March to 0.2. Than the tracer is mostly spread in the basin interior without a significant increase in maximal tracer surface concentration. From the TR2 distribution in winter-spring we can conclude that nutrients coming from the pool might contribute to the spring blooms mostly in the north Rim Current area and along the Anatolian coast. From September to November a strong increase of the surface tracer concentrations is simulated. A possible explanation of this occurrence includes amplification of the mesoscale circulations and the anticyclonic ones in particular. Typically in September lots of anticyclonic eddies are formed between the shelf edge and the Rim Current (Korotaev et al., 2003; Kubryakov, and Stanichny 2015; Miladinova et al., 2017). Formation and intensification of anticyclonic structures in the northern part (i.e. the Sevastopol eddy among others) are the key factors for the abrupt surface tracer increase in fall. Thus, our suggestions for the mechanisms of bloom formation during the winter cooling period are based on the development and strengthening of the mesoscale circulation in fall. It appears that the winter bloom does not due to the shallow position of the main pycnocline as supposed in Finenko et al. (2014). The wet phytoplankton biomass in February 1991 reached 100 g m^{-2} and the Chl in the mixed layer reached 2.6 μg l^{-1} (Mikaelyan, 1995). However, the area of this bloom was restricted to the northern part of the basin where there exists a strong interaction between the Rim current and anticyclonic eddies (e.g. the Sevastopol and Crimea) (Miladinova et al., 2017). The rapid uplift of tracer concentration in fall is also well visible in Fig. 7b, where the upper 10 m climatological tracer concentration averaged on the deep basin (depth > 1500 m) is shown. The

climatological distribution of the vertical TR2 contours in the deep basin is plotted in Fig. 7a.

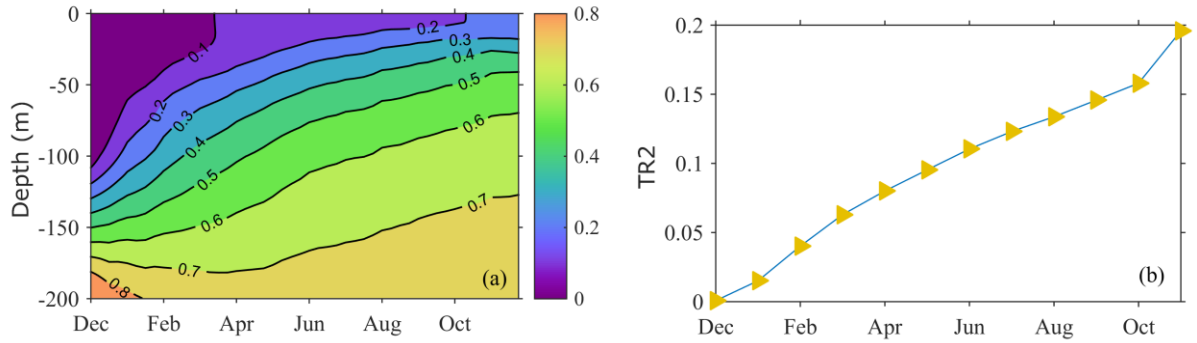

Figure 7. Deep basin (a) climatological vertical contours of TR2 and (b) upper 10 m climatological tracer concentration.

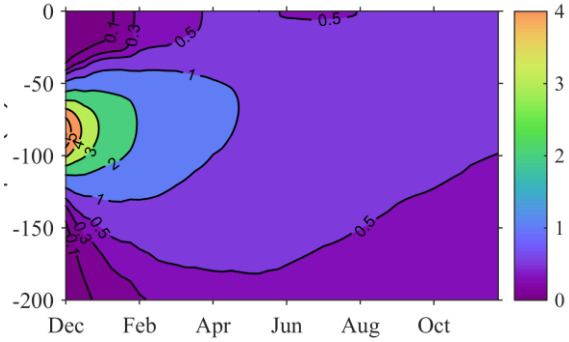

Figure 8. Deep basin climatological (for 1960-1990) vertical contours of TR3.

Nitrate is low in the euphotic zone due to biological uptake. It increases with depth as oxygen decreases due to nitrification. At the depth where oxygen has been reduced to low concentrations, nitrate reaches a maximum and then decreases sharply with depth. The linear decrease of nitrate with depth suggests that it distribution maybe diffusion controlled (Murray et al., 2005). Increases in the nitrate storage of the central basin after the 1960s have been documented by different groups (Codispoti et al., 1991; Konovalov and Murray, 2001; Tugrul et al., 1992). These changes are supposed to be due to increased nitrate loads of the major rivers with modified Si/N/P ratios (Cociasu et al., 1996; Oguz et al., 2008) and remineralisation of organic matter. The maximum nitrate concentration in the storage is observed in the late 1980–early 1990s (8 – 10 mmol N m^{-3}) when the riverine nutrient inputs are at maximum levels (Baştürk et al., 1998; Konovalov and Murray, 2001; Oguz et al., 2008). TR3 runs are designed to describe the mixing of the nitrate storage in winter. For the TR3 simulations the origin of nitrate storage is not important, since TR3 is initialised with the same profile (with a strong sub-surface maximum of about 8 mmol m^{-3}) in each December (see Fig. 3a for the tracer initial profile). Figure 8 shows vertical climatological TR3 contours averaged for the deep basin. The strong surface mixing in winter brings to the euphotic zone about 4% of the maximum tracer concentration (the initial maximum TR3 is 8 mmol m^{-3}). Despite the severity of the winter, the nitrate from the storage could not be completely mixed with the surrounding upper layers. This is because it occupies intermediate levels that include the CIL (upper part of the storage) and the main pycnocline (lower part that contains the maximum nitrate concentrations). Due to the permanent and strong stratification the surface mixed layer in winter does not reach the main pycnocline (Murray et al., 1991; Özsoy and

Ünlüata, 1997). Thus the TR3 indicates that the uplift of nitrate from the storage in February-April is a key factor for early spring phytoplankton bloom.

In summary, the three tracer simulations support the following hypotheses:

- Winter bloom is initiated by the uplift of nutrients from the basin pool in fall (TR2);
- Spring bloom is maintained by the winter surface mixing of the nitrate storage (TR3);
- Summer and fall blooms are sustained directly by the nutrient rich NWS waters (TR1).

3.1 Updated BSEM model calibration

The determination of key model parameters is still a work in progress. The working version of the BSEM parameterisation is given in Table 1. An example of the seasonal evolution of the surface chlorophyll estimated by the updated BSEM model is displayed in Fig. 9. We assume that the stoichiometric conversion of N to Chl - (mmol N m^{-3}):(mg Chl m^{-3})=1, and it remains unchanged despite the existing complexity. The chlorophyll is calculated as the sum of small and large phytoplankton which is converted from (mmol N m^{-3}) to (mg Chl m^{-3}). Our simulations show a strong winter (December-February) surface bloom of phytoplankton followed by a lower bloom in spring. Actually, we can suppose that the bloom starts in fall, than it is amplified in winter and calmed down in late spring. These occurrences are not in contradiction with other modelling studies and observational data (Oguz et al., 1999 and 2006; Vedernikov and Demidov, 1997).

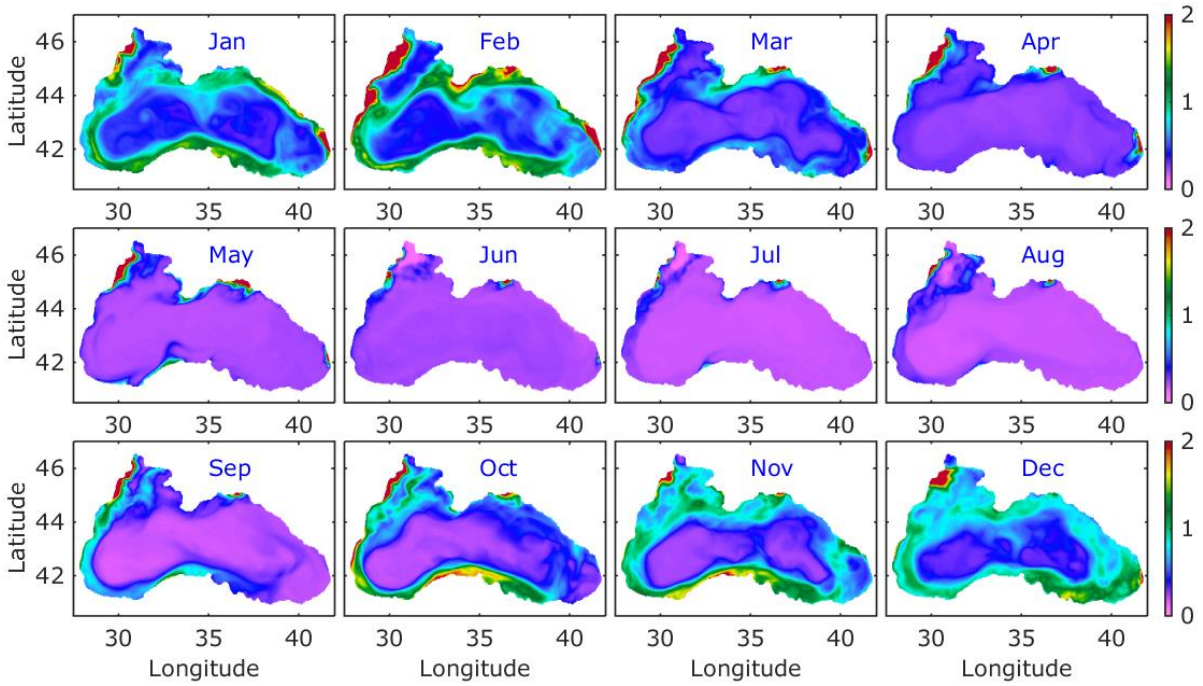

Figure 9. Monthly mean distribution of chlorophyll (mg Chl m^{-3}) in the surface 5 m for 1999 (updated BSEM simulations).

The phytoplankton concentration in the surface layer of the Rim current area is several times more than in the deep basin interior. It is worth to note that the western shelf and coastal areas exhibit elevated phytoplankton concentrations in the surface layers. Other area with very high phytoplankton concentrations includes the Anatolian shelf and coast. Satellite data (Fig. 10) shows similar occurrences. It is known that the standard NASA

algorithm overestimates Chl in the open waters of the Black Sea, thus in Fig. 10 is presented the Chl seasonal distribution acquired on the base of satellite data reanalysis and in Fig.11 – based on model results (CMEMS, http://marine.copernicus.eu). CMEMs model results are created by the MAST/ULg Production Unit by means of the GHER 3D circulation model online coupled with the BAMHBI biogeochemical model (Capet et al, 2016).

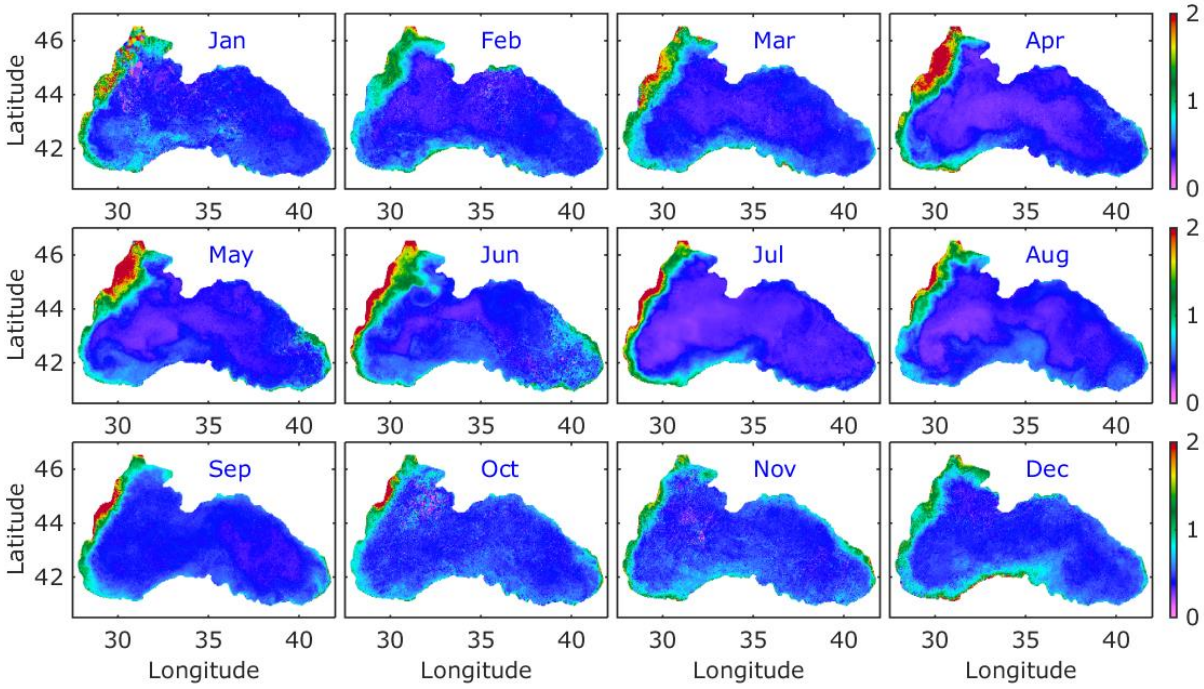

Figure 10. Monthly mean distribution of chlorophyll (mg Chl m^{-3}) from multi-satellite CMEMS reanalysis data for 1999.

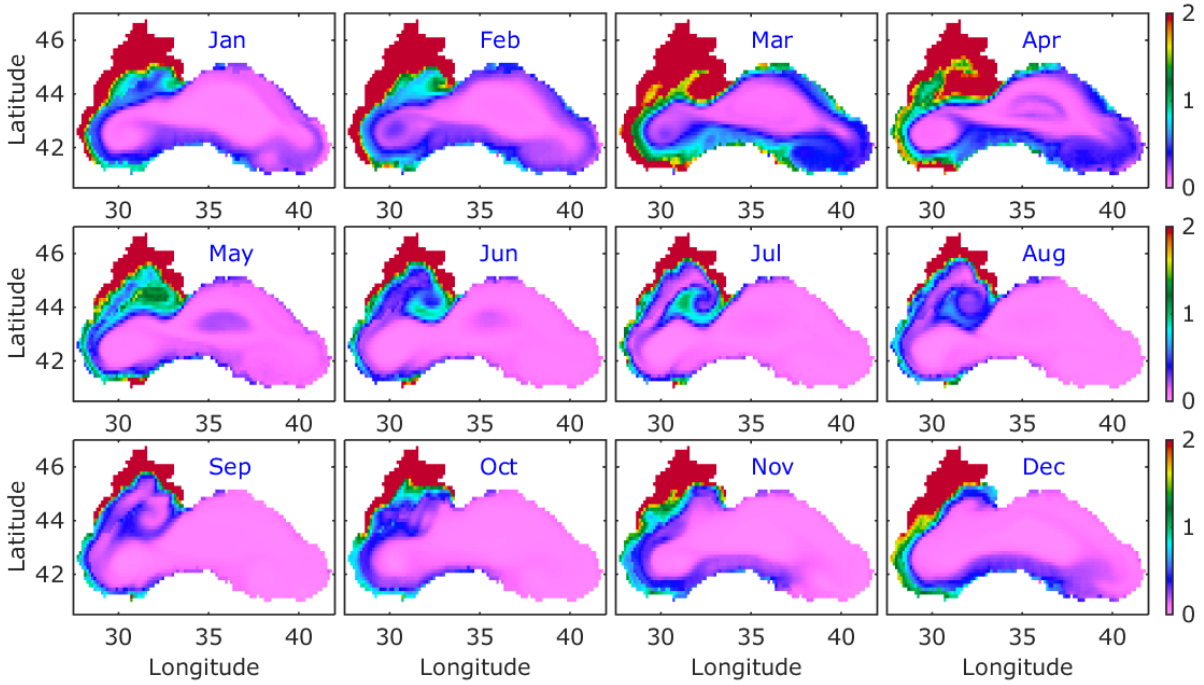

Figure 11. Monthly mean distribution of chlorophyll (mg Chl m^{-3}) from CMEMS model simulations for 1999.

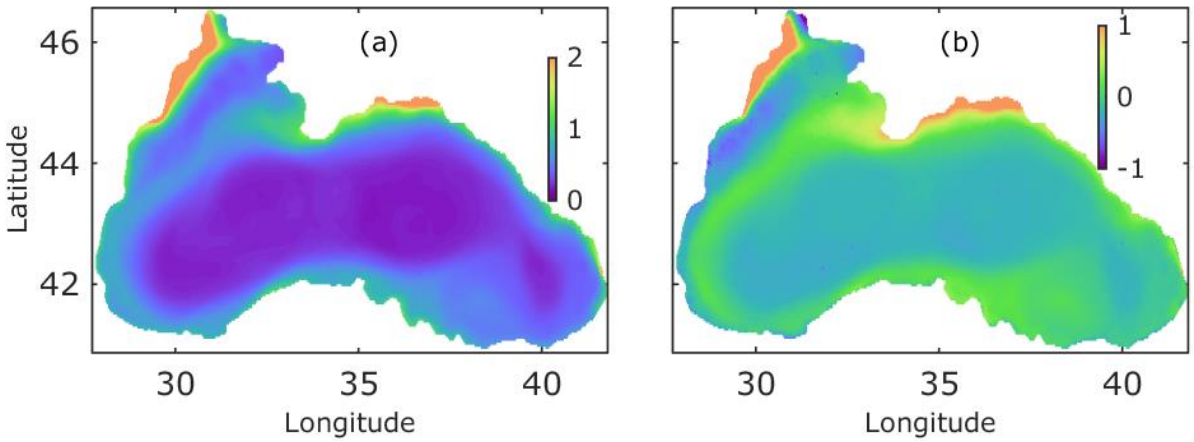

Figure 12. (a) Mean chlorophyll (mg Chl m^{-3}) over 1998 – 2002 calculated by the nitrate limiting version of BSEM. (b) Bias between BSEM model and CMEMS satellite climatology.

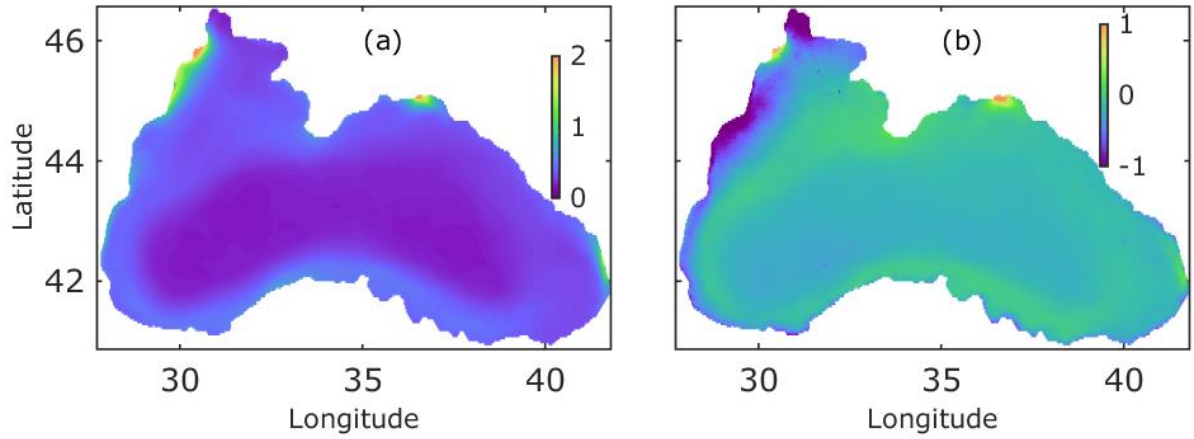

Figure 13. (a) Mean chlorophyll (mg Chl m^{-3}) over 1998 – 2002 calculated by the new nitrate-phosphate limiting version of BSEM. (b) Bias between the current BSEM model and CMEMS satellite climatology.

Simulations with the previous BSEM model reported higher chlorophyll concentrations along the shelf and lower in the basin interior (Fig. 12 a). It is worth to note the high chlorophyll in the Danube and Dniestr nearby zones and close to the Kerch Strait. The multi-annual (1998 – 2002) mean chlorophyll from multi-satellite CMEMS reanalysis, interpolated on the GETM domain, is extracted from the simulated multi-annual mean chlorophyll averaged over the same period (Fig. 12b). When model simulations are compared with the CMEMS satellite data, the BSEM model usually gives: a positive bias of about 0.5 mg Chl m^{-3} in the northern and southern shelf areas, as well as along Rim current meandering in the western basin; a negative bias in the western coastal areas and these close to the Danube, Dniestr and Dniepr river mouth; and the bias in the basin interior is almost negligible. In Fig. 13 are shown the same results as in Fig. 12 but found with the updated BSEM model. This model simulates less difference between areas confined by the Rim current and outside it. The overall bias with satellite reanalysis is lower, however the negative bias for the periphery of the western basin is raised.

4. Summary and conclusions

The present study makes use of tracer model simulations to describe several particular and important characteristic of the Black Sea flow and nutrient supply. Our simulations suggest the following features:

(1) The upper layers circulation system involved a complex flow structure that evolved intensification of the mesoscale circulation in fall. As a consequence nutrients from the deeper layers move up to the euphotic zone. We can conclude that this is the driving mechanism for the strong phytoplankton bloom in winter.

(2) February-March surface mixing of the nitrate storage upper layers with the surface waters sustain the winter bloom and initiate the spring one.

(3) Nutrient rich waters coming from the NWS are subjected to 2-4 months mixing and spreading through the basin. As a result, they can initiate the late spring or summer blooms.

The existing BSEM model is developed to involve phosphorus limitation of the phytoplankton growth and inconstant $N:P$ ratio. Several small model modifications are done as well. The model update is still in progress. First simulations indicate the need of the proposed modifications. For example, phytoplankton bloom in the western coastal and shelf zones is decreased and better agree with the satellite based results. Further model calibrations are necessary to match the observational data. Additionally, the improvement of the nutrient initial and forcing data is crucially important.

References

Artioli Y, Friedrich J, Gilbert JA, McQuatters-Gollop A, Mee DL, Vermaat EJ, Wulff F, Humborg C, Palmeri L, Pollehne F. 2008. Nutrient budgets for European seas: a measure of the effectiveness of nutrient reduction policies. Mar Pollut Bull 56:1609–1617

Baştürk, O., Turgul, S., Konovalov, S., Salihoglu, I., 1997. Variation in the vertical structure of water chemistry within the three hydrodynamically different regions of the Black Sea. In: Ozsoy, E., Mikaelyan, A. (Eds.), Sensitivity to Change: Black Sea, Baltic Sea and North Sea. NATO-ASI Series, Environment, 27. Kluwer Academic Publishers, Dordrecht, pp. 183–196.

Bruggeman, J. and Bolding, K. 2014. A general framework for aquatic biogeochemical models. Environmental Modelling and Software, 61, 249–265

Cannaby, H., Bettina A. Fach, Sinan S. Arkin, Baris Salihoglu, 2015. Climatic controls on biophysical interactions in the Black Sea under present day conditions and a potential future (A1B) climate scenario, Journal of Marine Systems 141, 149–166 doi:10.1016/j.jmarsys.2014.08.005

Capet A., Meysman, F., Akoumianaki, I., Soetaert, K. and Grégoire, M. 2016. Integrating sediment biogeochemistry into 3D oceanic models: A study of benthicpelagic coupling in the Black Sea. Ocean Modelling, 101, 83-100.

Cociasu, A., L. Dorogan, C. Humborg and L. Popa, 1996. Long-term ecological changes in the Romanian coastal waters of the Black Sea. Marine Pollution Bulletin, 32**,** 32–38.

Codispoti, L.A., Friederich, G.E.,Murray, J.W., Samatamota, C.M., 1991. Chemical variability in the Black Sea: implications of data obtained with a continuous vertical profiling system that penetrated the oxic/anoxic interface. Deep-Sea Res. 38 (Suppl. 2), 691–710.

Finenko, Z., Suslin, V., Kovaleva, I., 2014. Seasonal and long-term dynamics of the chlorophyll concentration in the Black Sea according to satellite observations. Oceanology 2014 (54), 596–605.

Galbraith E. D., and A. C. Martiny 2015, A simple nutrient-dependence mechanism for predicting the stoichiometry of marine ecosystems, PNAS | July 7, | vol. 112 | no. 27 | 8199–8204 www.pnas.org/cgi/doi/10.1073/pnas.1423917112

Kideys A.E., 2002 Ecology. Fall and rise of the Black Sea ecosystem. Science. 297(5586):1482-4. DOI:10.1126/science.1073002

Konovalov, S.K., Murray, J.W., 2001. Variations in the chemistry of the Black sea on a time scale of decades (1960–1995). Journal of Marine Systems 31 (1–3), 217–243.

Korotaev, G., T. Oguz, A. Nikiforov, and C. Koblinsky (2003), Seasonal, interannual, and mesoscale variability of the Black Sea upper layer circulation derived from altimeter data, J. Geophys. Res., 108, C43122, doi:10.1029/2002JC001508.

Kubryakov, A. A., and S.V. Stanichny (2015), Seasonal and interannual variability of the Black Sea eddies and its dependence on characteristics of the large-scale circulation, Deep-Sea Res. Pt. I, 97, 80-91, https://doi.org/10.1016/j.dsr.2014.12.002

Ludwig W, Bouwman AF, Dumont E, Lespinas F Water and nutrient fluxes from major Mediterranean and Black Sea rivers: Past and future trends and their implications for the basin - scale budgets, Global Biogeochem. Cycles, 24, GB0A13, (2010)

Martiny, A. C. et al. (2013), Strong latitudinal patterns in the elemental ratios of marine plankton and organic matter. Nature Geosci. 6, 279–283 http://dx.doi.org/10.1038/ngeo1757

Mee, L., 1992.The Black Sea in crisis: call for concerned international action. Ambio 21,278–286.

Mikaelyan, A.S., 1995. Winter bloom of the diatom *Nitzschia delicatula* in the open waters of the Black sea. Mar. Ecol. Prog. Ser. 129, 241–251.

Mikaelyan, A. S., Zatsepin, A. G., Chasovnikov, V.K., 2013. Long-term changes in nutrient supply of phytoplankton growth in the Black Sea. Journal of Marine Systems, Vol. 117-118: 53–64

Mikaelyan, A.S., Pautova, L.A., Chasovnikov, V.K., Mosharov, S.A., Silkin, V.A., 2015. Alternation of diatoms and coccolithophores in the northeastern Black Sea: a response to nutrient changes. Hydrobiologia 755, 89–105. http://dx.doi.org/10.1007/s10750-015-2219-z

Mikaelyan, A.S., Chasovnikov V. K., Kubryakov A. A., Stanichny S. V. 2017 Phenology and drivers of the winter–spring phytoplankton bloom in the open Black Sea: The application of Sverdrup's hypothesis and its refinements Progress in Oceanography, 151 163–176.

Miladinova, S., Stips, A., (2010) Sensitivity of oxygen dynamics in the water column of the Baltic Sea to external forcing. Ocean Sci. 6, 461-474. doi:10.5194/os-6-461-2010

Miladinova-Marinova S., A. Stips, E. Garcia-Gorriz, D. Macias Moy (2016a), Black Sea ecosystem model: setup and validation, EUR 27786, doi: 10.2788/601495

Miladinova S., A. Stips, E. Garcia-Gorriz, D. Macias Moy (2016b), Changes in the Black Sea physical properties and their effect on the ecosystem, EUR 28060, doi:10.2788/69832

Miladinova S., A. Stips, E. Garcia-Gorriz, D. Macias Moy (2016c), Modelling Toolbox 2: The Black Sea ecosystem model, EUR 28372 EN, doi:10.2788/677808

Miladinova S., A. Stips, E. Garcia-Gorriz, D. Macias Moy, (2017) Black Sea thermohaline properties: Long-term trends and variations, submitted in Journal of Geophysical Research - Oceans.

Moore, C. M. et al., (2013) - Mills, Processes and patterns of oceanic nutrient limitation, Nature Geoscience, 6, 701-710, http://dx.doi.org/10.1038/ngeo1765

Murray, J.W. (Ed.), Black Sea Oceanography. Deep-Sea Research II, vol. 53, pp. 1737–2004, 2006.

Murray, J. W., Z. Top, and E. Ozsoy, 1991 . Hydrographic properties and ventilation of the Black Sea. Deep-Sea Res., 38, Suppl.2A, S663–690

Nesterova, D., Moncheva, S., Mikaelyan, A.S., et al., 2008. The state of phytoplankton. In: Oguz, T. (Ed.), State of the Environment of the Black Sea (2001–2006/7). BSS, Istanbul, Turkey, pp. 173–192

Nezlin, N.P., 2008. Seasonal and interannual variability of remotely sensed chlorophyll. In: Kostianoy, G., Kosarev, A.N. (Eds.), The Handbook of Environmental Chemistry. Vol. 5, Part Q: The Black Sea Environment. Springer Verlag, Berlin-Heidelberg, pp. 333–349.

Oguz T. 2005 Long-Term Impacts of on the Black Sea Ecosystem, Oceanography, Vol.18, No.2

Oguz, T., H. Ducklow, P. Malanotte-Rizzoli, J.W. Murray, V.I. Vedernikov, and U. Unluata. , 2014 A physical-biochemical model of plankton productivity and nitrogen cycling in the Black Sea. Deep-Sea Res. I. 46, 597–636 , 1999

Oguz, T., Ducklow, H.W., and Malanotte-Rizzoli, P.: Modeling distinct vertical biogeochemical structure of the Black Sea: dynamical coupling of the oxic, suboxic and anoxic layers, Global Biogeochem. Cy., 14, 1331–1352, 2000.

Oguz, T., and D., Ediger 2006. Comparision of in situ and satellite-derived chlorophyll pigment concentrations, and impact of phytoplankton bloom on the suboxic layer structure in the western Black Sea during May–June 2001 Deep-Sea Research II 53, 1923–1933.

Oguz T., P.E. La Violette, Ü. Ünlüata, 1992 The upper layer circulation of the Black Sea: its variability as inferred from hydrographie and satellite observations. J. Geophys. Res., 97, CS, 12569-12584.

Oguz, T., Tugrul, S., Kideys, A.E., Ediger, V.and Kubilay, N., 2004 Physical and biogeochemical characteristics of the Black Sea (28,S), in: The Sea, vol. 14, edited by: Robinson, A. R. and Brink, K. H., Harvard University Press, chap. 33, 1331–1369.

Oguz T, and Merico A., 2006. Factors controlling the summer *Emiliania huxleyi* bloom in the Black Sea: a modelling study. J Mar Syst 59:173–188.

Oguz, T., B. Salihoglu, and B. Fach, 2008 A coupled plankton–anchovy population dynamics model assessing nonlinear controls of anchovy and gelatinous biomass in the Black Sea, Mar. Ecol. Prog. Ser. **369**, 229–256.

Oguz, T., Stips, A., Macias, D., Garcia-Gorriz, E. and Coughlan, C.: Development of the Black Sea specific ecosystem model (BSSM), Technical report, EUR27003EN, European Commission, Ispra, 2014.

Oguz T, Velikova V (2010) Abrupt transition of the northwestern Black Sea shelf ecosystem from a eutrophic to an alternative pristine state. Mar Ecol Prog Ser 405:231-242. https://doi.org/10.3354/meps08538

Özsoy, E., and Ü. Ünlüata (1997), Oceanography of the Black Sea: A review of some recent results, Earth. Sci. Rev., 42(4), 231–272

Pakhomova, S., E. Vinogradova, E. Yakushev, et al., "Interannual variability of the Black Sea proper oxygen and nutrients regime: the role of climatic and anthropogenic forcing," Estuarine, Coastal Shelf Sci. **140**, 134–145 (2014).

Paulmier, A., Kriest, I., and Oschlies, A.: Stoichiometries of remineralisation and denitrification in global biogeochemical ocean models, Biogeosciences, 6, 923–935, 2009, http://www.biogeosciences.net/6/923/2009/

Silkin, V.A., Pautova, L.A., Pakhomova, S.V., Lifanchuk, A.V., Yakushev, E.V., Chasovnikov, V.K., 2014, Environmental control on phytoplankton community structure in the NE Black Sea, Journal of Experimental Marine Biology and Ecology, Volume 461, Pages 267-274, https://doi.org/10.1016/j.jembe.2014.08.009

Sorokin, Y.I., 2002. The Black Sea ecology and oceanography. Backhuys Publishers, Leiden, 875 pp.

Stanev, E., He, Y., Staneva, J. and Yakushev, E. , 2014 Mixing in the Black Sea detected from the temporal and spatial variability of oxygen and sulfide – Argo float observations and numerical modelling, Biogeosciences, 11, 5707–5732

Teng, Y., Primeau, F. W., Moore, J. K., Lomas, M. W. & Martiny, A. C. Global-scale variations of the ratios of carbon to phosphorus in exported marine organic matter. Nature Geosci. 7, 895–898 (2014)

Tsiaras, K. P., V. H. Kourafalou, A. Davidov, and J. Staneva (2008), A three-dimensional coupled model of the western Black Sea plankton dynamics: Seasonal variability and comparison to SeaWiFS data, J. Geophys. Res., 113, C07007, doi:10.1029/2006JC003959.

Tugrul, S., Murray, J. W., Friederich, G. E., and Salihŏglu, I. , 2014. Spatial and temporal variability in the chemical properties of the oxic and suboxic layers of the Black Sea, J. Marine Syst., 135, 29–43.

Vedernikov, V.I. and A.B. Demidov, 1997. Vertical distributions of primary production and chlorophyll during different seasons in deep part of the Black Sea, Oceanology, 37**,** 376-384.

Yunev O. A., J. Carstensen, S. Moncheva, et al., 2007. Nutrient and Phytoplankton Trends on the Western Black Sea Shelf in Response to Cultural Eutrophication and Climate Changes. Estuar.Coast.ShelfSci.74, 63–76.

Yunev,O., Velikova V., Carstensen J. 2017. Reconstructing the trophic history of the Black Sea shelf. Continental Shelf Research, 150, 1-9. http://dx.doi.org/10.1016/j.csr.2016.08.008i

Wroblewski, J. (1977), A model of phytoplankton plume formation during variable Oregon upwelling, J. Mar. Res., 35, 357– 394.

List of abbreviations and definitions

BSEM: Black Sea Specific Ecosystem Model
CIL: Cold Intermediate Layer
ECMWF: European Center for Medium Range Weather Forecast
ERA40: ECMWF ERA 40 reanalysis
ERA-interim: ECMWF ERA-interim reanalysis
EU: European Union
FABM: Framework for Aquatic Biogeochemical Models
GRDC: Global River Data Center database
GETM: General Estuarine Ocean Model
JRC: Joint Research Centre
MC: Marie Curie
ML: Mixed layer
MEDAR/MEDATLAS: Mediterranean Data Archaeology and Rescue database
MSFD: Marine Strategy Framework Directive
N: Nitrogen
P: Phosphorus
SIMSEA: Scenario simulations of the changing Black Sea ecosystem
SeaWiFS: Sea viewing Wide Field of view Sensor
HS: Hydrogen sulphide
SST: Sea surface temperature

List of figures

List of tables

How to obtain EU publications

Our publications are available from EU Bookshop (http://bookshop.europa.eu),
where you can place an order with the sales agent of your choice.

The Publications Office has a worldwide network of sales agents.
You can obtain their contact details by sending a fax to (352) 29 29-42758.

KJ-NA-28983-EN-N

JRC Mission

As the Commission's in-house science service, the Joint Research Centre's mission is to provide EU policies with independent, evidence-based scientific and technical support throughout the whole policy cycle.

Working in close cooperation with policy Directorates-General, the JRC addresses key societal challenges while stimulating innovation through developing new methods, tools and standards, and sharing its know-how with the Member States, the scientific community and international partners.

Serving society
Stimulating innovation
Supporting legislation

Publications Office

doi: 10.2760/220233

ISBN 978-92-79-77212-2